The International Journal of Advanced Manufacturing Technology (2019) 101:243–259
https://doi.org/10.1007/s00170-018-2868-y

ORIGINAL ARTICLE

Consistent kinematics and dynamics calibration of lightweight redundant industrial manipulators

Sergey Kolyubin[1] · **Anton Shiriaev**[2] · **Anthony Jubien**[3]

Received: 16 March 2018 / Accepted: 8 October 2018 / Published online: 31 October 2018

Abstract

Absolute accuracy is one of industrial manipulator's key performance characteristics, which is critical for emerging robotics applications such as laser cutting, riveting, and carbon fiber placement as well as for many machining operations. On the other hand, arrival of new uses such as collaborative robots needs the estimation of interaction efforts with the operator or with the environment (hand-guiding, collision detection, and free backlash assembly). This paper presents an approach to organize an integrated kinematic and dynamic calibration procedure to improve quality of models appropriate for trajectory planning and motion control. Along with bringing theoretical insights and novel arguments, we give hands-on recommendations on selection of parameters priors, initial guesses on calibration poses and trajectories, setting active constraints, algorithms tuning, and experimental data filtering which is necessary to perform consistent robot calibration in practice. We illustrate the study with experimental data and description of actual calibration performed on the KUKA Light-Weight Robot using vision-based metrology and dedicated software. In contrast to authors preceding works, this paper includes a more complete entire procedure description, analysis of dynamic calibration sensitivity with respect to kinematic parameters estimates and a chapter on how calibration results can be used for model-based trajectories planning using virtual holonomic constraints approach.

Keywords Industrial manipulator · Robot calibration · Collaborative robots · Redundant kinematics · Dynamics identification · Optimization methods

1 Introduction

Erroneous estimates of robot parameters used by a motion planner or a controller can significantly degrade an overall system performance. Thereby, one of prerequisites for such applications is a properly organized and implemented calibration procedure. However, this task is rarely completely automated. In most cases, in order to arrive to consistent results, standard identification approaches and computational schemes require tuning, supervision, and manual adjustments [20]. An expert should categorize which effects can have the major influence on the robot for expected operations and which can be disregarded trading-off between the model complexity and its relevance to a behavior that the real system will perform. In doing so, s/he typically decides on a number of degrees of freedom that is sufficient for representing a particular motion of the robot, on kinematic and dynamic features of an end-effector, and on a necessity to include in analysis properties of actuators and transmissions. S/he scrutinizes characteristics of measurement instruments available for recording robot's motion and

The work of S. Kolyubin is supported by the Russian Science Foundation grant (project No.17-79-20341).

Electronic supplementary material The online version of this article (https://doi.org/10.1007/s00170-018-2868-y) contains supplementary material, which is available to authorized users.

✉ Sergey Kolyubin
s.kolyubin@corp.ifmo.ru

Anton Shiriaev
anton.shiriaev@ntnu.no

Anthony Jubien
anthony.jubien@hestiam.com

[1] School of Computer Technologies and Control, ITMO University, 197101 St. Petersburg, Russia

[2] Department of Engineering Cybernetics, NTNU, NO-7491 Trondheim, Norway

[3] Nantes Digital Sciences Laboratory – LS2N, 44300 Nantes, France

tunes various filters and observers for recovering signals impossible to measure directly. For instance, if an expected motion is relatively slow, then one may require accurate friction models and observers for reconstructing velocities of related coordinates to compensate detrimental effects of such forces [9]. On the other hand, if an expected motion is relatively quick, then one might need to increase a number of degrees of freedom to capture non-negligible links and joints flexibility [29].

Usually, kinematic and dynamic calibration tasks are treated separately. The first one represents the task to identify kinematic parameters of a manipulator typically required to reach a maximal accuracy in positioning of its tool for point-to-point motions and assumes the presence of an external measurement device that can be used for validation of *an absolute location of a robot's tool in the world frame.* While the second one is aimed at developing an accurate dynamic model appropriate either for rigorous simulation and trajectories planning or for high-performance control, when, for instance, a robot is to be programmed to follow a time-optimal behavior with demanding velocity and acceleration profiles. It relies on a measurement system of the robot and, therefore, serves primarily for the internal representation of trajectories and feedback design strategies. The translation of the robot motion from its internal representation into a task -specific coordinate system is left as a minor step in the majority of the dynamics calibration case studies. At the same time, interference from the robot incorrect kinematics representation on its dynamic model identification both at the calibration trajectories planning and parameters calculation steps was reported in previous research (e.g. [37]).

This work describes analytic, computational, and experimental steps implemented for estimating kinematic and dynamic parameters of a robot equipped with an advanced research interface for signal acquisition and control used together with an advanced metrology instrument and dedicated software for tracking robot behaviors in the world frame.

Namely, the discussed calibration procedure has been implemented on the KUKA Light-Weight Robot (LWR4+), which is a redundant serial manipulator with seven rotational joints. Its attractive features such as kinematics redundancy and joint torque sensing as well as real-time control capabilities provided via the Fast Research Interface (FRI) [3] have helped the robot to serve as one of popular and widely used platforms in robotics research specifically for developing and testing new motion planning and motion control algorithms. Being appropriate for some assignments, parameters of a robot extracted from its CAD model require refinements for others tasks, where by necessity an experimenter should take into account neglected or averaged effects due to motors' dynamics, friction, non-uniform mass distribution of links, and robot-to-robot variations.

Apart from the manipulator, the robotic cell under the study has been equipped with the Nikon K610 optical coordinate measuring machine (CMM). The advanced software tools enables their synchronization resulting in tracking of a selected frame's origin and orientation at the sampling rate of 1 kHz and with the volumetric accuracy of 60 μm over a workspace of 17 m^3.

The rest of the paper is organized as follows. The next section highlights the novelty and contribution of this study, particularly addressing the difference between this work and other researchers and authors previous publications. Sections 3 and 4 are devoted to kinematics and dynamics calibration respectively, where we added formal problem statements and analytic and experimental steps in their solutions. In Section 4.5 the case study setup and the realization of generic arguments for identification of its Inverse Dynamic Models (IDMs) are presented. Section 5 presents a comment for model-based trajectory planning based on the developed IDMs. Finally, discussion on the obtained results and concluding remarks are given in Section 6 and Section 7 respectively.

2 Novelty and contribution

To the best of authors knowledge, there are no works focused on integrated identification of the robot kinematic and dynamic models; therefore, the suggested procedure has scientific novelty and is technically sound. Consistency between geometric and inertial parameters estimates can be important for the case study and in general for model-based optimal trajectories planning and motion control, since the latter depend on the former in a nonlinear way, and erroneous guesses on robot geometry can propagate while capturing its dynamic behavior [37]. Analysis of dynamic calibration results' sensitivity with respect to kinematic parameters estimates and more complete entire procedure discussion including a chapter on how calibration results can be further used for trajectories planning bring value to this paper with respect to authors' preceding works [26–28].

Here, we can also highlight authors' contribution compared to other state-of-the-art techniques for kinematics and dynamics calibration separately.

Despite kinematics calibration is a well-established field of research [10, 14, 15, 18, 21, 22], its further development is motivated by many practical applications [6–8, 30, 31].

The kinematics calibration part of this work is based on the general framework introduced in [22], but also employs recent findings in the calibration configurations optimization such as meta-heuristic search algorithms [8]

as well as suggests an alternative approach for preventing sticking in a local minimum given a non-convex cost function corresponding to various observability indexes [15] by introducing a multi-start optimization approach. Similar to [34], authors consider calibration using vision-based metrology with target full-pose measurements by means of a fixed exteroceptive sensor. However, authors used a photogrammetry setup with three linear charge-coupled device (CCD) cameras; therefore, a novel target design was introduced and poses optimization procedure was modified with Cartesian-space constraints to ensure target and base frames visibility during the experiment. In terms of implementation, we proposed a highly automated procedure specifically adapted for the optical CMM use.

The dynamics calibration part of this paper tries to address the problem in its full complexity considering advanced model reduction for complete links and motor dynamics and ways to provide convergence of parameters estimates under noisy measurements by means of trajectories planning, signal processing, and estimation algorithm adjustments. These issues have been addressed by other researchers as well, but from different angles and/or often in fragmented fashion. Since there are many works on robot dynamics identification in recent years, we mention here only those mostly devoted to parametric estimation (not frequency-domain methods) and redundant serial kinematics manipulators as a case study.

For example, works [2, 37] consider only link dynamics neglecting motor dynamics. Calibration trajectories are parametrized by Fourier series, while its desired frequencies and amplitudes are calculated using d-optimality criterion. No model reduction approach is considered, instead a full barycentric parameters set is used. While [37] presents results for six degrees of freedom (DOF) articulated robot, similar approach is applied to 7DOF KUKA LWR manipulator in [2].

Identification of the KUKA LWR dynamics is accomplished in [11] using a reverse engineering approach, i.e., mapping numerical values of the link inertia matrix and the gravity vector with the proposed symbolic model at a set of static configurations. This work considers recursive model for link dynamics neglecting friction terms. During the calibration experiment, all robot joints were requested to move along the same non-optimized periodic single frequency trajectory, while the position measurements were numerically differentiated and low-pass filtered. This study reports that the proposed approach provides poor accuracy in the computed torque test for the joints that are less loaded.

Work [25] suggests a closed-form solution for identification model reduction, which allows selecting a set of base inertial parameters by converting observation matrix to the reduced-row echelon form. It allows to find transformation matrix in a symbolic form, which is different from often used QR or singular vector decomposition (SVD) numeric approaches. Future possible identification model reduction based on confidence of obtained parameters estimates is not considered here.

Works [12, 36] consider the problem of mapping between recursive model dynamic coefficients and physical robot parameters. Both works are considering link dynamics only. Stürz et al. [36] are introducing additional constraints on link physical parameters at the step of dynamic coefficients identification to make its estimates feasible. It is also referring to model reduction, but up to base parameters set only, and to excitation trajectories planning, which is based on a single-criterion optimization. Gaz et. al [12] focus on recovering values of link masses, inertia tensors, and center of gravity (CoG) coordinates from the obtained numerical estimates of dynamic coefficients using optimization procedures. In contrast, our work shows that physical parameters values may be not needed for a trajectories planning algorithm.

Similar to our work, [33] addresses the problem of handling measurements noise, while organizing the identification procedure, and in particular at the excitation trajectories planning step by improving signal-to-noise ratio. However, this work proposes to apply single-criterion optimization, when the cost function is defined as the sum of two scalar functions, where the first summand is an observation matrix condition number and the second one is the reciprocal of the sum of the joint torques for all joints over pre-selected points of the trajectory. This approach does not allow targeting torques of particular (e.g., poorly loaded) joints. B-spline parametrization of excitation trajectories is suggested, which allows adjusting trajectories locally without affecting the rest of the path. However, these trajectories are not periodic and are not explicitly parametrized with respect to motion frequencies.

Works [5, 16, 17] are the closest to the dynamic calibration part of this study in terms of the model and signal processing algorithms used as well as experimental setup under consideration. However, it suggests to use non-optimized calibration trajectories with trapezoidal velocity profile, which can significantly deteriorate estimation quality. In our study, we enhanced the approach from [17] and proposed multi-objective optimization settings for searching robot's calibration trajectories. As shown, the adjustment resulted in trajectories with better excitation of dynamics of the last joints and consequently helped to improve accuracy of parameters estimates. The similarity with [17] in modeling the dynamics and in description of a set of essential parameters allowed for the case study organizing the comparative analysis of the robot-to-robot variations. Besides that various hands-on recommendations on selection of parameters priors, initial guesses on calibration poses and trajectories, setting active constraints, algorithms tuning,

and experimental data filtering are provided throughout the paper.

3 Steps in kinematics calibration

Below we describe and comment on steps necessary for kinematics calibration giving guidelines on making choices for (1) a parametric family of robot models, (2) one or several optimization indexes and algorithms for searching an optimal set of calibration configurations, and (3) computational algorithm for estimating robot geometric parameters. We illustrate study with experiments for the KUKA LWR4+ robotic arm.

3.1 Kinematics model for calibration

We consider a serial open-chain redundant manipulator and assume that the robot is rigid and flexibility in links and transmission are negligible. Thus, no degrees of freedom, in addition to joint angles, will be introduced for kinematics modeling. Under these conditions, the posture $\boldsymbol{y} = [x, y, z, \phi, \theta, \psi]^T$ of a robot end-effector with $[x, y, z]$ being Cartesian coordinates and with $[\phi, \theta, \psi]$ being tool central point (TCP) frame orientation in the world frame can be obtained from the forward kinematics equations

$$\boldsymbol{y} = f(\boldsymbol{\Phi}, \boldsymbol{q}), \tag{1}$$

where $\boldsymbol{q} = [q_1, \ldots, q_n]^T$ is a vector of joint coordinates that uniquely determine the robot configuration and $\boldsymbol{\Phi}$ is a vector of unknown geometric parameters.

For a robot consisting of n joints and $n+1$ links, the transformation from the robot base to its terminal link coordinate frames assigned using modified Denavit-Hartenberg (MDH) convention [20, 23] can be expressed as

$$^0T_n(\boldsymbol{q}) = {}^0T_1(q_1) \cdot {}^1T_2(q_2) \cdot \ldots \cdot {}^{n-1}T_n(q_n), \tag{2}$$

where each element in the product is given by

$$^{j-1}T_j = \mathrm{Rot}_x(\alpha_j)\mathrm{Trans}_x(d_j)\mathrm{Rot}_z(\theta_j)\mathrm{Trans}_z(r_j)$$

and represents a transformation between two consecutive link frames calculated for quadruples of geometric parameters $(\alpha_j, d_j, \theta_j, r_j)$.

For the calibration task, we introduce two additional coordinate frames representing camera frame indexed as -1 and tool frame indexed as $n+1$ (see Fig. 1).

Since these frames can be arbitrarily located in space, then, in general, up to six parameters $(\gamma_z, b_z, \alpha_z, d_z, \theta_z, r_z)$ may be required for defining a transformation $({}^{-1}T_0)$ between the camera and robot base frames and another six values $(\gamma_e, b_e, \alpha_e, d_e, \theta_e, r_e)$ for a transformation $({}^nT_{n+1})$ between the robot terminal link and tool frames. However, taking into account properties of the robot terminal and base frames, one can introduce these transformations in the unified with Eq. 2 manner:

$$\begin{aligned} {}^{-1}T_1(\boldsymbol{q}) &= {}^{-1}T_0 \cdot {}^0T_1(q_1) \\ &= \mathrm{Rot}_x(\alpha_0)\mathrm{Trans}_x(d_0)\mathrm{Rot}_z(\theta_0)\mathrm{Trans}_z(r_0) \\ &\quad \times \mathrm{Rot}_x(\alpha_1')\mathrm{Trans}_x(d_1')\mathrm{Rot}_z(\theta_1')\mathrm{Trans}_z(r_1'), \end{aligned} \tag{3a}$$

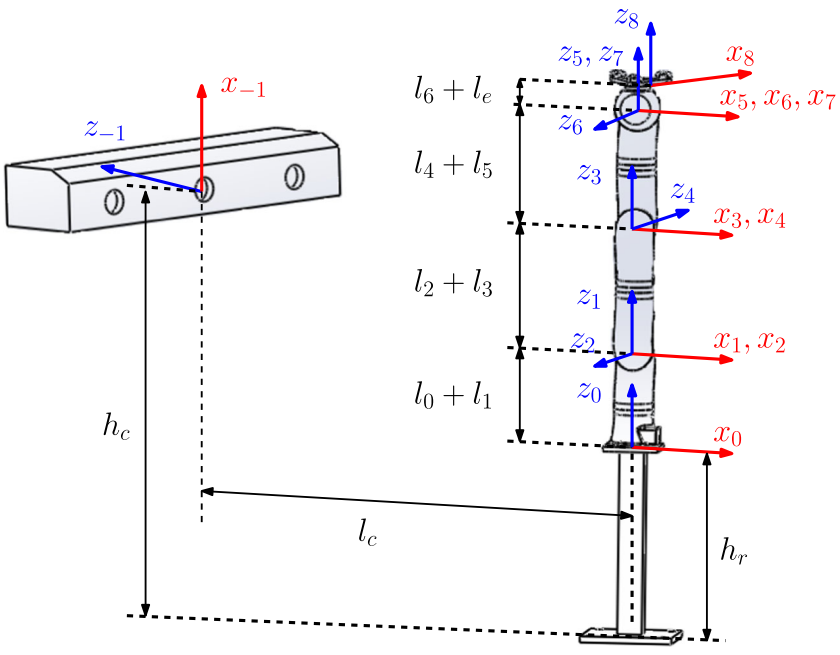

Fig. 1 Camera, robot, and tool frames assignment

where $\alpha_0 = 0, d_0 = 0, \theta_0 = \gamma_z, r_0 = b_z, \alpha'_1 = \alpha_z, d'_1 = d_z, \theta'_1 = \theta_1 + \theta_z, r'_1 = r_1 + r_z$, and

$$\begin{aligned} {}^{n-1}T_{n+1}(\boldsymbol{q}) &= {}^{n-1}T_n(q_n) \cdot {}^{n}T_{n+1} \\ &= \mathrm{Rot}_x(\alpha_n)\mathrm{Trans}_x(d_n)\mathrm{Rot}_z(\theta'_n)\mathrm{Trans}_z(r'_n) \\ &\quad \times \mathrm{Rot}_x(\alpha_{n+1})\mathrm{Trans}_x(d_{n+1})\mathrm{Rot}_z(\theta_{n+1})\mathrm{Trans}_z(r_{n+1}), \end{aligned} \tag{3b}$$

where $\theta'_n = \theta_n + \gamma_e, r'_n = r_n + b_e, \alpha_{n+1} = \alpha_e, d_{n+1} = d_e, \theta_{n+1} = \theta_e, r_{n+1} = r_e$.

Augmenting Eq. 2 with Eqs. 3a and 3b, we obtain forward kinematics equations

$${}^{-1}T_{n+1}(\boldsymbol{q}) = {}^{-1}T_0 \cdot {}^{0}T_n(\boldsymbol{q}) \cdot {}^{n}T_{n+1}, \tag{4}$$

which can be used for computing the posture of the end-effector as defined by Eq. 1. In this case, a vector of unknown parameters in the representation (1) becomes

$$\Phi = \left[\alpha'_1, \ldots \alpha_{n+1}, d'_1, \ldots d_{n+1}, \theta_0, \ldots \theta_{n+1}, r_0, \ldots r_{n+1}\right].$$

3.2 Goal of kinematics calibration

Given an estimate $\hat{\Phi}$ of the vector Φ and Eq. 1, a pose $\boldsymbol{y}$ of the robot's end-effector can be pre-computed by the formula

$$\hat{\boldsymbol{y}} = f(\hat{\Phi}, \boldsymbol{q}) \tag{5}$$

simultaneously for all feasible robot configurations $\boldsymbol{q}$ at once. Therefore, one can justify the closeness of $\hat{\Phi}$ to Φ implicitly by comparing values of the pre-computed $\hat{\boldsymbol{y}}$ and measured $\boldsymbol{y}$ end-effector's poses for different configurations $\boldsymbol{q}$. It is common to assume that an estimate $\hat{\Phi}$ of MDH parameters reproduces the true one, if the corresponding pre-computed pose $\hat{\boldsymbol{y}}$ and its "ground-truth" value $\boldsymbol{y}$ are indistinguishable for any choice of $\boldsymbol{q}$. The statement admits the reformulation as a solution of an optimization task

$$\hat{\Phi}_{opt} := \arg \min_{\forall \boldsymbol{q}} \|\boldsymbol{y} - \hat{\boldsymbol{y}}\|^2. \tag{6}$$

The problem can have many local minima; therefore, the vector $\hat{\Phi}_{opt}$ in Eq. 6 denotes a global optimizer. For the most of robot designs, it is sufficient to use a finite number M of configurations $\boldsymbol{q}$ in searching of $\hat{\Phi}_{opt}$ provided that a set of these configurations $\{\boldsymbol{q}^1, \ldots, \boldsymbol{q}^M\}$ is chosen properly and the constrained optimization task

$$\hat{\Phi}_{opt}(q^1, \ldots, q^M) := \arg \min_{\boldsymbol{q} \in \{\boldsymbol{q}^1, \ldots, \boldsymbol{q}^M\}} \|\boldsymbol{y} - \hat{\boldsymbol{y}}\|^2 \tag{7}$$

returns the global optimizer $\hat{\Phi}_{opt} \equiv \hat{\Phi}_{opt}(\boldsymbol{q}^1, \ldots, \boldsymbol{q}^M)$.

If the vector Φ possesses parameters that are not identifiable from the output $\boldsymbol{y}$, then the parametrization is excessive and a set of redundant characteristics should be found. In practice, such parameters can be singled out analyzing the so-called *parametric Jacobian*

$$J(\boldsymbol{q}) = \frac{\partial f(\Phi, \boldsymbol{q})}{\partial \Phi}. \tag{8}$$

Indeed, if $J(\cdot)$ is insensitive to some parameters in Φ for any configuration $\boldsymbol{q}$, then these parameters would be challenging to identify. Typically, they are either eliminated from the model or regrouped with others. The remaining set of identifiable parameters and the corresponding parametric Jacobian are called *base parameters* Φ_B and *base Jacobian* $J_B(\boldsymbol{q})$ respectively (see [14, 20, 22]).

3.3 Algorithms and heuristics for searching optimal calibration configurations

The process of selecting a set of robot configurations $Q = \{\boldsymbol{q}^1, \ldots, \boldsymbol{q}^M\}$ for the optimization task (7) and steps in selecting the base parameters Φ_B of the forward kinematics (4) of the robot become interconnected if one considers and explores the so-called *base observation matrix*

$$W_B(Q) := \left[\, J_B(\boldsymbol{q}^1)^T,\ J_B(\boldsymbol{q}^2)^T,\ \ldots,\ J_B(\boldsymbol{q}^M)^T \,\right]^T \tag{9}$$

Its maximal rank indicates a number of identifiable (base) parameters, while the corresponding set Q describes configurations, which the robot should visit in experiment. Frankly speaking, one can choose arbitrarily many configurations $\boldsymbol{q}^i$ in Q. However, in the design of experiments, it is reasonable to limit a number of configurations and choose them wisely. As quantitative measures of the configurations optimality, several *observability indexes* $O(Q)$ and associated optimization assignments were discussed in [8, 14, 15]. Essentially, they explore and rely on the SVD decomposition of the base Jacobian $J_B(\boldsymbol{q})$ and the results can be interpreted as searching for a set of configurations, for which end-effector poses are sensitive to small perturbations of the base parameters. Thus, optimizing a set of configurations Q can be formulated as a maximization of a selected observability index subject to nonlinear constraints

$$\max_{Q=\{q^1, q^2, \ldots q^M\}} O(Q) \quad \text{such that} \quad \begin{cases} q^l \in (q_{\min}, q_{\max}), \\ y^l \in (y_{\min}, y_{\max}), \end{cases} \quad l = 1, 2, \ldots, M. \tag{10}$$

Here, sub-indexes max and min denote maximum and minimum allowed values respectively. The constraints listed in the optimization problem (10) are given both in the joint and in the Cartesian spaces. The latter can be present, if there are obstacles inside the robot's workspace or there are specifications imposed due to basic principles of measurement instruments. For instance, if the photogrammetry technology is applied, then the problem formulation should include end-effector visibility constraints.

A common practice in calibration poses' optimization is to use the conjugate-type deterministic algorithm [20, 22]. It is aimed at adjusting the entire set of configurations on every iteration. However, such algorithm has a number of deficiencies including its strong dependence on initial conditions and a possibility to converge to one of local minima. To avoid the issues, we tested two modifications: The first one performs a multi-start procedure assuming that the algorithm is run several times from randomly chosen and uniformly distributed set of initial conditions. In the second modification, we tested an Iterative Meta-Heuristic Algorithm with the Tabu Rule (IMHATR) [8], which runs as a two-stage procedure illustrated by Fig. 2. Here, the Tabu list T is a set of already verified configurations introduced to prevent convergence to one of known local minima. This scheme is similar to a genetic algorithm, where a stochastic behavior is introduced at the randomized candidate-configurations selection step. The results and discussions of the comparative analysis of different observability indexes and poses optimization algorithms can be found in [26, 28].

3.4 Geometric parameters estimation

When a set of robot configurations for minimizing the index (7) is successfully determined, a numerical procedure for computing its global optimizer Φ_{opt} can be initiated and implemented in various ways. In this work we realized the classical *iterative linear least squares* algorithm

$$\Delta Y_k = Y_m - F(\hat{\Phi}_{k-1}, Q), \tag{11a}$$

$$\Delta \Phi_{B,k} = W_B^+ \Delta Y_k, \tag{11b}$$

$$\hat{\Phi}_{B,k} = \hat{\Phi}_{B,k-1} + \Delta \Phi_{B,k}. \tag{11c}$$

Here, W_B^+ is the pseudo-inverse of the base observation matrix W_B defined in (9); $Y_m = \left[\boldsymbol{y}_m^1; \boldsymbol{y}_m^2; \dots \boldsymbol{y}_m^M\right]^T \in \mathbb{R}^{6M}$ and $F(\hat{\Phi}_k, Q) = \left[f(\hat{\Phi}_k, \boldsymbol{q}^1); \quad f(\hat{\Phi}_k, \boldsymbol{q}^2); \dots f(\hat{\Phi}_k, \boldsymbol{q}^M)\right] \in \mathbb{R}^{6M}$ denote respectively vectors of measured (1) and calculated (5) tool frame positions and orientations aggregated for a set of M configurations of the set Q; an index k corresponds to kth iteration. Elements of $\hat{\Phi}_k$ corresponding to the base parameters are updated from $\Phi_{B,k}$, while others are kept equal to its initial values.

In addition, the *Levenberg-Marquardt* or *damped least-squares* algorithm was also implemented to improve a convergence if the second-order terms of the Taylor series expansion of Eq. 11a were significant

$$\Delta \Phi_{B,k} = \left[W_B^T W_B + \lambda_k \mathrm{diag}\left(W_B^T W_B\right)\right]^{-1} W_B^T \Delta Y_k. \tag{12}$$

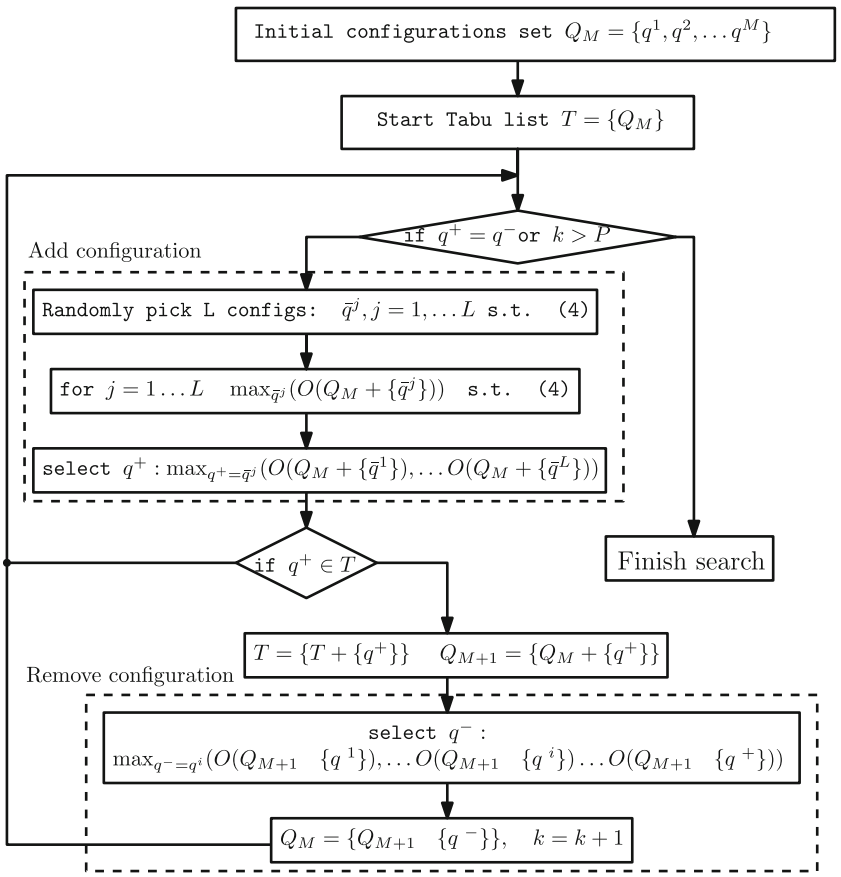

Fig. 2 Diagram for IMHATR algorithm

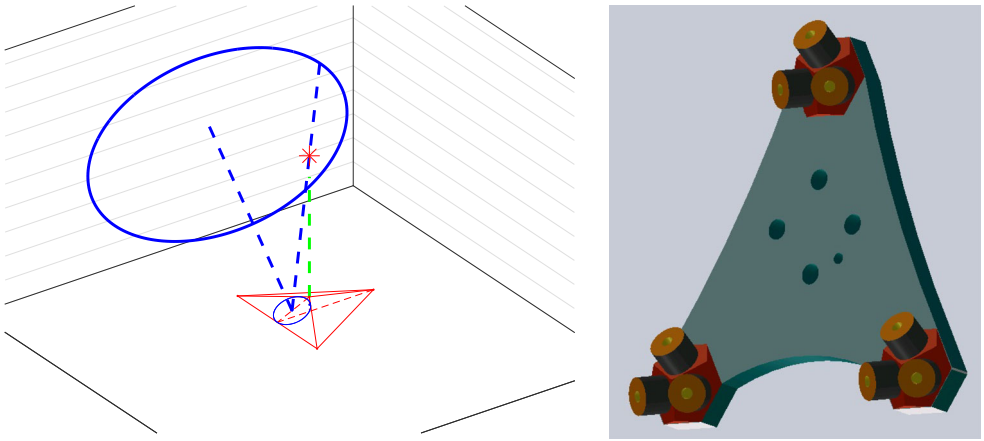

Fig. 3 LED fixture design

Here, ΔY_k is calculated as in Eq. 11a and the non-negative damping factor λ_k is adjusted at each iteration following the heuristics:

- if $\|\Delta Y_{k+1}\| < \|\Delta Y_k\| \quad \Rightarrow \quad \lambda_{k+1} = \lambda_k/10$
- else $\quad \lambda_{k+1} = 10 \cdot \lambda_k$

3.5 Experiment organization

For kinematics calibration, we used Nikon K610 optical CMM that provides position and orientation measurements for dynamically moving frames.

In order to organize measurements, two frames were marked for the CMM with two sets of LEDs—the robot base frame and the tool frame. The former was assigned to compensate for possible camera relocation between series of experiments and allowed us to directly measure relative full pose between two aforementioned frames.

To ensure better visibility and localization accuracy for the tool frame, we designed a special LED fixture that was attached to the robot flange (see Fig. 3). Reasoning behind the fixture geometry is explained in [28].

Table 1 contains the list of active constraints imposed on joint angles and tool pose in Cartesian space with respect to the camera frame to guarantee the LED visibility and avoid collisions.

For optimizing calibration configurations, *Matlab Optimization Toolbox* was used. The selection of base parameters and the calculation of their estimates were implemented in the software package *GECARO+* [24]. FRI was used to control the robot motion during experiments. In order to operate the K610 CMM, to assign dynamic frames, and to acquire measurements via the DMM-Modular protocol, Nikon Metrology's *K-CMM*, *DMM*, and *Geoloc* software were used.

The process of the kinematics calibration is illustrated in the supplementary multimedia file.

4 Steps in dynamics calibration

In this section, we provide background, describe step-by-step procedure, and point out adjustments essential for accurate open-chain manipulator dynamics recovering. Results presented in this section are recalling approaches described in authors' previous work [27], while its extension in terms of comprehensive analysis on how preliminary kinematic calibration and calibration trajectories planning influence dynamic model identification are presented in Section 6.2.

4.1 Dynamics model for calibration

The dynamics of an open-chain manipulator with n-degrees of freedom and physically collocated actuators having substantial gear-ratios in transmission[1] can be well approximated by the Inverse Dynamics Model (IDM)

$$\tau_l = M(q)\ddot{q} + C(q,\dot{q})\dot{q} + G(q) + \tau_{fl}, \tag{13}$$

$$\tau = I_a\ddot{q} + \tau_l + \tau_{fm}. \tag{14}$$

Here, q, $\dot{q}$, and $\ddot{q} \in \mathbb{R}^n$ are vectors of joint positions, velocities, and accelerations; τ and $\tau_l \in \mathbb{R}^n$ are vectors of motor and joint torques; $M(q)$ is $n \times n$ link inertia matrix; $C(q,\dot{q})\dot{q}$ and $G(q) \in \mathbb{R}^n$ are vectors representing Coriolis/centrifugal generalized forces and forces due to gravity or compliance; I_a is the diagonal drive inertia matrix (motor and gearbox); and τ_{fm} and $\tau_{fl} \in \mathbb{R}^n$ are vectors of motor and joint friction torques.

[1] According to DLR Light-Weight Robot III specifications http://www.dlr.de/rmc/rm/en/desktopdefault.aspx/tabid-3803/6175_read-8963/ (the predecessor of the KUKA LWR4+), all seven harmonic drives have high gear ratios. In particular, they are 1:100 for axes 1, 2, 3, 4, 6, and 7 and 1:160 for axis 5.

Table 1 Constraints for configurations optimization

Joint angles, [rad]	$\lvert q_{1,3,5,7}\rvert \le \frac{17\pi}{18}$; $\lvert q_{2,4}\rvert \le \frac{2\pi}{3}$; $\lvert q_6\rvert \le \frac{\pi}{2}$
LED fixture orientation in camera frame, [rad]	Roll $\phi \in \left[-\frac{4\pi}{9}, \frac{7\pi}{18}\right]$; pitch $\theta \in \left[-\frac{\pi}{4}, \frac{\pi}{4}\right]$
LED fixture position in robot base frame, [rad]	Distance in XY plane $d_{xy} \ge 0.2$; Vertical coordinate $z \ge -0.1$

The identification task requires also a parametrization of dissipative generalized forces represented in Eqs. 13 and 14 in the lump format as torques τ_{fl} and τ_{fm}. The simplest parametric model of a friction includes symmetric and decoupled Coulomb and linear viscous parts solely dependent on links' angular velocities

$$\tau_{fl} = F_{vl}\dot{q} + F_{cl}\mathtt{sign}(\dot{q}) + offl, \tag{15}$$

$$\tau_{fm} = F_{vm}\dot{q} + F_{cm}\mathtt{sign}(\dot{q}) + offm. \tag{16}$$

Here, F_{vm}, F_{cm}, F_{vl}, and F_{cl} are $n \times n$ diagonal constant matrices of viscous and Coulomb friction coefficients for motors and joints respectively; $offm$ and $offl \in \mathbb{R}^n$ are motor and joint torque offsets.

As known from [10, 14, 20], nonlinear Eqs. 13–16 of the robot dynamics can be transformed into a recursive dynamic model, which is linear in unknown barycentric parameters

$$\tau(t) = \omega\left(q(t), \dot{q}(t), \ddot{q}(t)\right)\chi, \quad \forall t. \tag{17}$$

The $[n \times N_s]$ matrix function $\omega(\cdot)$ represents the *IDM Jacobian* with respect to a vector of parameters $\chi = [\chi_1; \ldots; \chi_n] \in \mathbb{R}^{N_s}$, where each column has seventeen elements $\chi_j = [XX_j,\ XY_j,\ XZ_j,\ YY_j,\ YZ_j,\ ZZ_j,\ MX_j,\ MY_j,\ MZ_j,\ M_j, I_{aj},\ F_{vl,j},\ F_{cl,j},\ offl_j,\ F_{vm,j},\ F_{cm,j},\ offm_j]^T$ with $XX_j, XY_j, XZ_j, YY_j, YZ_j$, and ZZ_j being the inertia tensors, MX_j, MY_j, and MZ_j being the first moments, M_j being the mass all listed for the jth link, $j = 1, \ldots, n$, and with $N_s = 17 \cdot n$ being the total number of barycentric parameters.

The representation (17) is often redundant and some of parameters might not be identifiable. Therefore, similar to Section 3, one searches for a subset of n_b *base IDM parameters* χ_B with $n_b \le N_s$, which are sufficient for reconstructing the motors' torques in the left-hand-side of Eq. 17

$$\tau(t) = \omega_B\left(q(t), \dot{q}(t), \ddot{q}(t)\right)\chi_B, \quad \forall t. \tag{18}$$

Here, $\omega_B(\cdot)$ known as the *base IDM Jacobian* $[n \times n_b]$ matrix is composed from n_b columns of $\omega(\cdot)$ originally defined by the dynamics in Eq. 17. Sets of base parameters can be determined using closed-form rules of [22] or QR-decomposition of the IDM Jacobian (see [21]). In turn, some of the base IDM parameters might not have a significant contribution to the system dynamics and can be post-eliminated reducing a set of the base parameters to a smaller set of *essential IDM parameters*. Systematically, it can be done using statistical hypothesis tests [16]. However, if identification steps for both motor and joint dynamics are performed concurrently, then one needs to keep among essential parameters those which can be only estimated in hard-to-excite modes. In this case, a manually supervised iterative elimination procedure can be implemented as an alternative [20].

4.2 Signal processing and additional model transformations

Motivated by practical use, several additional assumptions and transformations of the model (18) are necessary.

The *first* one is related to representation of a noise that appears in measurements of $q(\cdot)$, $\tau(\cdot)$ and enters into coefficients of the regressor $\omega_B(\cdot)$. The common approach is to neglect the measurement's noise in computing $\omega_B(\cdot)$ and assume that the following model reproduces the measurements accurately

$$\tau(t) = \omega_B\left(q(t), \dot{q}(t), \ddot{q}(t)\right)\chi_B + \epsilon(t), \tag{19}$$

i.e., the noise $\epsilon(t)$ is additive. If such assumption is accepted, then collecting measurements, while the robot is moving along a certain trajectory, and augmenting the data results into the over-determined set of linear equations

$$\Upsilon = \Omega_B\chi_B + E, \tag{20}$$

where Υ and E are the vectors of "stacked" actual motor torques and model errors respectively, all of a size $[r \times 1]$ with $r = n \cdot n_e$ and n_e being the number of measurement samples; Ω_B is the *IDM observations matrix* vertically stacked from $\omega_B\left(q(t_k), \dot{q}(t_k), \ddot{q}(t_k)\right)$ blocks for $k = 1, \ldots, n_e$, [16].

The *second* assumption characterizes results of pre-processing of raw measurements of $\tau(\cdot)$ and $q(\cdot)$ for reducing noise and for estimating velocities and accelerations required in computing the regressor. It is commonly done by band-pass filtering of all signals resulting into the Inverse Dynamic Identification Model (IDIM)

$$\Upsilon_f = \Omega_{Bf}\chi_B + E_f, \tag{21}$$

where the index f denotes filtered data

$$\Upsilon_f = \left[\tau^f(t_1); \tau^f(t_2); \ldots \tau^f(t_{n_e})\right],$$

$$\Omega_{Bf} = \begin{bmatrix} \omega_B\left(\hat{q}^f(t_1), \hat{\dot{q}}^f(t_1), \hat{\ddot{q}}^f(t_1)\right) \\ \vdots \\ \omega_B\left(\hat{q}^f(t_{n_e}), \hat{\dot{q}}^f(t_{n_e}), \hat{\ddot{q}}^f(t_{n_e})\right) \end{bmatrix}.$$

Then, the *second* assumption postulates that the filtered error signal E_f in Eq. 21 has zero mean, serially uncorrelated and heteroskedastic [16]. It implies that E_f has a block-diagonal covariance matrix

$$R = \text{diag}\left(\sigma_1^2\mathbf{I}_{ne}, \cdots, \sigma_j^2\mathbf{I}_{ne}, \cdots, \sigma_n^2\mathbf{I}_{ne}\right), \tag{22}$$

where I_{ne} is the $[n_e \times n_e]$ identity matrix and σ_j^2 is the error variance calculated from jth subsystem of Eq. 21.

4.3 Searching for optimal calibration trajectories

Successful identification of robot's dynamics relies on availability of a family of rich-in-modes robot's nominal trajectories $q_i^*(\cdot)$. Performing them in experiments generates input data for computing estimates of model parameters based on the linear regression (18) or its filtered version (21). For various reasons, it is convenient to consider a parametric family of nominal trajectories, where behaviors of joint coordinates are trigonometric polynomials of time, i.e., when the motion of ith joint ($i = 1, \ldots, n$) is written as

$$q_i^\star(t) = q_{i,0} + \sum_{k=1}^{n_f}\left[a_{i,k}\sin\left(k \cdot w_0 t\right) + b_{i,k}\cos\left(k \cdot w_0 t\right)\right]. \tag{23}$$

Here, $q_{i,0}$ is the initial bias, w_0 is the base frequency, $a_{i,k}$ and $b_{i,k}$ are constant coefficients, and n_f is the number of frequencies.

Searching coefficients $\left\{a_{i,k}, b_{i,k}\right\}$ of trigonometric polynomials (23) is commonly done through solving appropriately posted constrained optimization task. Meanwhile, the order n_f of polynomials, their base frequency w_0 are often selected in advance: They should respond to requirements for inducing high-frequency modes ($w_0 \uparrow, n_f \uparrow$) and for covering a larger part of the robot workspace ($w_0 \downarrow$). However, they cannot be any and, in particular, to avoid an excitation of a hidden dynamics in transmission, the parameters should be consistent with the inequality $n_f \cdot w_0 < w_r$, where w_r is the smallest resonance frequency among the joints.

Some of constraints for optimization can be taken directly from the list of robot specifications representing limits imposed on joints' variables and their velocities. Others, such as geometrical constraints representing conditions for obstacle avoidance, self-occlusion and imposed in the workspace of the robot, require volumetric characteristics of a robot structure combined with the forward kinematics of the robot discussed on the previous step of the calibration process. Another important constraints, such as torques limits, require an iterative use of the model (13)–(16) with the current update of parameters available to the moment. Additional constraints can be enforced due to implementation conditions, e.g., zero joints' velocities and accelerations at the beginning and the end of a searched motion.

In order to achieve a coherent distribution of behaviors among joints, one can follow the common strategy and consider the optimization index defined as the condition number of the IDM observation matrix $\Omega_B(\cdot)$, i.e., $\texttt{cond}\left(\Omega_B\right) \rightarrow \min$. However, such choice might lead to trajectories with lack of sufficient excitation of weakly loaded wrist joints and bad signal-to-noise ratios of recorded data and potentially result in inaccurate estimates for their dynamic parameters. This is the case for the KUKA LWR4+ and we have tested the applicability of *multi-objective optimization* as one of alternatives for exciting the dynamics of the last two joints. The formal settings of such optimization assignment have been the following:[2]

$$\min_{\substack{q_{i,0}\\ a_{i,k},b_{i,k}}} \gamma \quad \texttt{s.t.} \begin{cases} F\left(q_{i,0}, a_{i,k}, b_{i,k}, t\right) - \gamma \cdot \Psi \le \Lambda, \\ \left[\dot{q}_i^\star(0),\ \ddot{q}_i^\star(0)\right] = [0,\ 0], \\ q_i^\star(t) \in (q_{i,min}, q_{i,max}), \\ \dot{q}_i^\star(t) \in (\dot{q}_{i,min}, \dot{q}_{i,max}), \\ \tau_i^\star(t) \in (\tau_{i,min}, \tau_{i,max}), \\ i = 1 \ldots n, \quad k = 1 \ldots n_f \\ d_{xy}(t) \ge 0.3,\ z(t) \ge -0.2. \end{cases} \tag{24}$$

Here, $\Lambda = \left[g_{\Omega_b}; k_{\tau_6} \cdot \tau_{6,max}; k_{\tau_7} \cdot \tau_{7,max}\right]$ is the goal matrix, γ is the attainment coefficient, $\Psi = |\Lambda|$ is the weight matrix, and

$$F(\cdot) = \left[\texttt{cond}\left(\Omega_B\right); \overline{\left(\tau_{6,max} - |\tau_6^\star(t)|\right)}; \overline{\left(\tau_{7,max} - |\tau_7^\star(t)|\right)}\right]$$

can be interpreted as the vector objective function, where $\overline{(\cdot)}$ denotes a mean value[3] of an argument over time-interval it is defined. The goal matrix parameters g_{Ω_b}, k_{τ_6}, and k_{τ_7} can largely affect the optimization results and should be carefully selected. A way to find their initial approximates is to perform a single criterion optimization (such as $\texttt{cond}\left(\Omega_B\right) \rightarrow \min$) in advance.

4.4 Parameters estimation and quality of estimates

In these settings, the optimal-in-variance estimates for elements of the vector χ_B are provided by the Weighted Least Squares (WLS) algorithm [14, 16, 17]

$$\hat{\chi}_B = \left(\Omega_{Bf}^T R^{-1} \Omega_{Bf}\right)^{-1} \Omega_{Bf}^T R^{-1} \Upsilon_f. \tag{25}$$

[2] The problem is specified in a form adapted for implementation with the Matlab "*fgoalattain*" function.

[3] Values for limits of joint angles, velocities, and torques can be found in the KUKA LWR4+ data-sheet.

The covariance matrix of such estimate given by $\Sigma = \left(\Omega_{Bf}^T R^{-1} \Omega_{Bf}\right)^{-1}$ quantitatively describes the parametric uncertainty in $\hat{\chi}_B$ as a whole, while the *relative standard deviation* (RSD) of the ith element in $\hat{\chi}_B$

$$\%\bar{\sigma}_{\hat{\chi}_B^i} = \frac{100 \cdot \bar{\sigma}_{\hat{\chi}_B^i}}{\left|\hat{\chi}_B^i\right|}, \tag{26}$$

can be used as a certificate for each individual characteristic, where $\bar{\sigma}^2_{\hat{\chi}_B^i}$ is the i-th diagonal coefficient of Σ.

Additional metrics for quality estimation results are

- physical feasibility of obtained parameters estimates;
- discrepancies between measured and recovered joint torques obtained as a result of computed-torque test.

Remark 1 The approach allows an efficient software realization of the identification procedure; however, the justification of the validity of the assumptions that support the method should be clearly performed in each case study. In general, they are met provided that measurements $q(\cdot)$ and $\tau(\cdot)$ are acquired at high sampling rate and the data filtering is well tuned.

4.5 Experiment organization

All the generic arguments for modeling and identification discussed above were applied for reconstructing dynamic models of the KUKA LWR4+ installed at the Industrial Robotics Lab, NTNU. For consistency of identification results, experiments were prepared and run on the original KUKA LWR4+ and on the robot equipped with additional payload firmly attached to the last joint. The payload was $\approx$ 3.28[kg] with an off-set of the center of mass away from the axis of rotation of joint 7 (see Fig. 4). In modeling and identification processes, it was treated as the link 8 fixed to the link 7 of the robot.

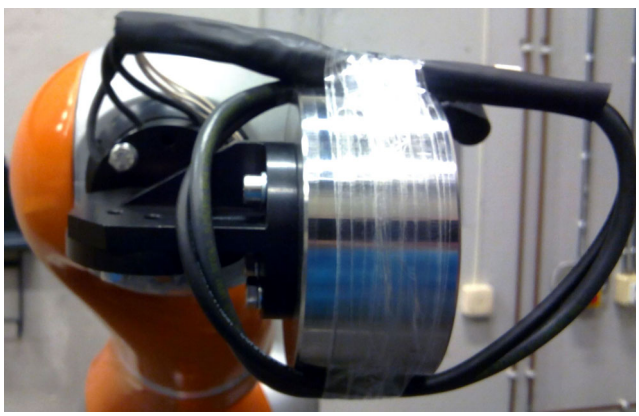

Fig. 4 Load for dynamics identification

The *Symoro+* package [19] was used both for dynamic model symbolic representations and for the automatic selection of its base parameters. The developed symbolic representations were exported to Matlab using the 'Optimizer' function of Symoro+ and further used in planning of excitation trajectories and in computing estimates for essential parameters.

The set of kinematic and dynamic constraints used at the calibration trajectories planning step is listed in Table 1.

Pre-computed trajectories were used for conducting a series of identification experiments. In doing so, we commanded reference trajectories by activating the LWR4+'s *joint position control mode*. Reflexxes On-Line Motion Library available via Stanford FRI Library[4] was used to generate smooth trajectories from an arbitrary pose to a start pose of the excitation trajectory.

"*Recorder*" function provided by KUKA was utilized to acquire motor and joint positions, motor currents and joint torques sampled at 1 kHz and to save logs with up to 60 s of records for each experiment. In order to prepare the acquired data for computing estimates of essential parameters, measured signals were pre-processed by the fourth-order band-pass Butterworth and the decimate filters with cutting-off frequencies of 10 Hz and 2 Hz respectively.

A reader can observe some of recorded experiments from the supplementary multimedia file.

5 IDIM for VHC-based trajectories planning and tracking

Most of modern feed-forward and feedback control methods utilized in robotics (such as PD+ with gravity compensation, inverse dynamics control, passivity based control etc.) rely on nominal representations of robot dynamics. Hence, reconstructing essential parameters of the IDM of a robot provides an analytic tool for developing model based motion and trajectory planning algorithms as well as control architectures.

In order to illustrate another application and another use of a reconstructed dynamics for a robot-manipulator, let us re-consider the classical approach of [4, 13] for planning time optimal behaviors of the system subject to velocity constraints.

The method assumes that a temporal behavior of all n-degrees of freedom of the robot (13) is parametrized through kinematic relations

$$q_1(t) = \phi_1(\theta(t)), \quad \ldots, \quad q_n(t) = \phi_n(\theta(t)), \tag{27}$$

where $\Phi(\cdot) = [\phi_1(\cdot), \ldots, \phi_n(\cdot)]^T$ are smooth functions, while the temporal behavior of the scalar variable $\theta(\cdot)$ is

[4] http://cs.stanford.edu/people/tkr/fri/html/index.html

defined to accommodate some specifications. Geometrically functions $\phi_i(\cdot)$ help to represent a path in a configuration space of the robot for searching a time-optimal behavior written in terms of an auxiliary variable $\theta(\cdot)$ introduced instead of time. It is common to assume that functions $\phi_i(\cdot)$ depend on a finite set of parameters that can be tuned in optimization. Such cascaded representation is convenient in re-writing any velocity limit imposed on a rate of change of a coordinate as a constraint on dynamics of $\theta(\cdot)$. Indeed, the implication

$$|\dot{q}_i(t)| = |\phi_i'(\theta(t))\dot{\theta}(t)| \le C_i \quad \Rightarrow \quad |\dot{\theta}(t)| \le \frac{C_i}{|\phi_i'(\theta(t))|}$$

gives the background for converting a generic velocity constraint in the system into the corresponding property imposed only on $\theta(\cdot), \dot{\theta}(\cdot)$ variables and parameters of $\phi_i(\cdot)$ functions. As known [4, 13], dynamics of the variable $\theta(\cdot)$ for the fully actuated case is determined by the equation

$$\alpha(\theta)\ddot{\theta} + \beta(\theta)\dot{\theta}^2 + \gamma(\theta) = u, \tag{28}$$

where the scalar functions $\alpha(\cdot)$, $\beta(\cdot)$, and $\gamma(\cdot)$ are computed from the dynamics of the robot and the choice of functions $\phi_i(\cdot)$; $u(\cdot)$ is a scalar control input, which might also depend on dissipative forces present in the dynamics of the robot. In examples, this equation is derived from (13) for given analytic expressions of the inertia matrix $M(\cdot)$, the Coriolis/centrifugal $C(\cdot)\dot{q}$, and the potential generalized forces $G(\cdot)$.

Indeed, the representation of the robot dynamics (13) for a motion, for which the relations (27) are invariant, takes the vector format

$$\tau_g = A(\theta)\ddot{\theta} + B(\theta)\dot{\theta}^2 + \Gamma(\theta), \tag{29}$$

with $\tau_g = \tau - \tau_{fm} - \tau_{fl}$, $A(\theta) = [\alpha_1(\theta) \dots \alpha_n(\theta)]^T$, $B(\theta) = [\beta_1(\theta) \dots \beta_n(\theta)]^T$ and $\Gamma(\theta) = [\gamma_1(\theta) \dots \gamma_n(\theta)]^T$.

Then, any linear combination of rows in Eq. 29 will result in Eq. 28.

The proposed dynamics calibration procedure suggests an alternative direct method for computing all the terms in Eq. 29 as functions of the IDM base Jacobian $\hat{\omega}_B(\cdot)$ and IDM base parameters estimates $\hat{\chi}_B$, which avoids reconstructing the matrix functions $\hat{M}(\cdot)$, $\hat{C}(\cdot)$, and $\hat{G}(\cdot)$.

Proposition 1 *Any motion of a system described by Euler-Lagrange equations (13) consistent with the kinematic relations (27) can be represented by (29) with coefficients that can be calculated as follows*

$$\Gamma(\theta) = \hat{\omega}_B(\theta, 0, 0)\,\hat{\chi}_B, \tag{30}$$

$$B(\theta) = \hat{\omega}_B(\theta, 1, 0)\,\hat{\chi}_B - \Gamma(\theta), \tag{31}$$

$$A(\theta) = \hat{\omega}_B(\theta, 1, 1)\,\hat{\chi}_B - B(\theta) - \Gamma(\theta). \tag{32}$$

Here, $\hat{\omega}_B(\cdot)$ and $\hat{\chi}_B$ correspond to the IDM base Jacobian and the IDM base parameters vector excluding terms related to friction.

Remark 2 Friction coefficients $offm$, $offl$, Fcm, Fcl, Fvm, and Fvl can always be identified separately from other base IDM parameters. Therefore, we can always find relations for $\hat{\omega}_B(\cdot)$ and $\hat{\chi}_B$ by excluding corresponding rows and components of $\omega_B(\cdot)$ and χ_B respectively.

Proof After path variable θ was introduced, we can define relations for reference trajectories of Eq. 13 in terms of joint coordinates, velocities, and accelerations

$$q^\star = \Phi(\theta), \quad \dot{q}^\star = \Phi'(\theta)\dot{\theta}, \quad \ddot{q}^\star = \Phi''\dot{\theta}^2 + \Phi'\ddot{\theta}, \tag{33}$$

where $\Phi(\theta)$ is the vector function in Eq. 27. Substituting relations from Eqs. 18 to 33, we derive

$$\tau^\star = \omega_B\left(\theta, \dot{\theta}, \ddot{\theta}\right)\chi_B. \tag{34}$$

Thus, at each time instance, we can calculate system dynamics along any reference trajectory $(q^\star, \dot{q}^\star, \ddot{q}^\star)$ based on Eqs. 30–32 and given parameters estimates $\hat{\chi}_B$. □

6 Discussion

6.1 Kinematics calibration results

The analysis of the robot parametric Jacobian showed that parameters α_0, d_0, θ_7, and r_7 should be eliminated as non-identifiable and the set of base parameters Φ_B consists of 32 elements. For optimizing a set of configurations, the observability index $O(Q)$ in Eq. 10 was chosen equal to the condition number of the base observation matrix $O(Q) := cond\,(W_B(Q))$. Numerical optimization resulted in 17 optimal configurations, for which $O(Q)$ achieves its minimal value equal to $\min O(Q) = 11.1878$.

For more details on calibration poses optimization using different observation indexes and algorithms, a reader can refer to authors' previous papers [26, 28].

Both the linear least-squares and Levenberg-Marquardt parameter estimation algorithms gave very similar results. The fact supports an applicability of the linear model, see also Eq. 11a,

$$\Delta Y = W_B(Q)\Delta\Phi_B, \tag{35}$$

in the identification of the KUKA LWR4+ redundant kinematics.

Values for nominal versus calibrated MDH parameters of the system are collected in Table 2. The data collected in Table 3 emphasize the positive effect of calibration by

Table 2 Nominal vs. calibrated MDH parameters

Frame	α_i [rad]		d_i [m]		θ_i [rad]		r_i [m]	
	nom.	calibr.	nom.	calibr.	nom.	calibr.	nom.	calibr.
0	0	0	0	0	1.55	1.5493	−4.3	−4.4066
1	1.5	1.5273	0.1	0.0698	$q_1 - 0.79$	$q_1 - 0.7994$	−0.14	−0.1375
2	$\pi/2$	$\pi/2 + 1.2 \cdot 10^{-4}$	0	−0.0003	q_2	$q_2 - 0.0042$	0	$3.9{\cdot}10^{-5}$
3	$-\pi/2$	$-\pi/2 + 6.1 \cdot 10^{-4}$	0	−0.0003	q_3	$q_3 - 0.0098$	0.4	0.3999
4	$-\pi/2$	$-\pi/2 + 1.4 \cdot 10^{-4}$	0	0.0011	q_4	$q_4 - 0.0065$	0	$2.6{\cdot}10^{-4}$
5	$\pi/2$	$\pi/2 - 1.1 \cdot 10^{-4}$	0	−0.0009	q_5	$q_5 + 0.0011$	0.39	0.3908
6	$\pi/2$	$\pi/2 + 6.4 \cdot 10^{-4}$	0	0.0004	q_6	$q_6 - 0.0016$	0	$1.6{\cdot}10^{-4}$
7	$-\pi/2$	$-\pi/2 - 3.6 \cdot 10^{-4}$	0	−0.0006	q_7	q_7	0	0
8	0	$5.30 \cdot 10^{-4}$	0.0015	−0.0002	0.79	0.7859	0.093	0.0911

comparing some of recorded end-point localization errors for nominal and calibrated MDH parameters.

6.2 Dynamics calibration results

Similar to [17], we considered three models for identification:

- Model 1 captures primarily the robot dynamics neglecting the dynamics of motors, i.e. Eq. 14 is replaced by the identity $\tau = \tau_l$ and corresponds to Model B in [17]. The approach is appropriate when measurements of joints' torques are only available and when motors' parameters are out of interest in application.
- Model 2 captures both links and motors dynamics, i.e., the IDM is calculated for the complete set of Eqs. 13–16, which correspond to Model C in [17]. The model assumes that motors and joints torques' measurements are both available.
- Model 3 captures the motors' parameters appeared in Eqs. 14 and 16 and corresponds to Model D in [17].

Identifying such model requires both motor and joint torque measurements, but, in contrast to Model 2, it relies on difference between these signals. Such approach allows estimating parameters of the motors dynamics gained independently of properties of the robot dynamics.

Table 3 End-point positioning volumetric deviations

Parameters set	Position [mm]		Orientation [deg]	
	max	Average	max	Average
Nominal	9.6806	5.9019	0.8058	0.5636
Calibrated	1.7592	0.7965	0.2268	0.1042

Remark 3 Structurally, the model (13)–(14) for the KUKA LWR4+ is not new and has been used in [17], but it differs from the parametric representation of the KUKA LWR4+ dynamics considered in [11], where the coupling of the robot and motor dynamics were described through the deflection model and Hooke's law.

For example, for the most complete Model 2 written originally with $136 (= 8 \cdot 17)$ IDM parameters (for 7 joints and a payload) the *Symoro+* package [19] found *eighteen* non-identifiable parameters and suggested other *sixteen* to be regrouped resulting altogether in the set of *base parameters* with 102 elements. *Forty four* of them were later singled out by the manually supervised iterative procedure as *essential* [5]. Regrouping relations for base parameters were similar to ones reported in [17, Table III].

Planning of excitation trajectories for the derived symbolic representations of Models 1–3 was approached and reformulated as constrained optimization problems for searching coefficients of polynomials (23) in two different settings:

- Trajectory A is calculated as a result of the single-objective optimization $\mathtt{cond}\,(\Omega_B) \rightarrow \min$;
- Trajectory B is calculated as a result of the multi-objective optimization (24) with $g_{\Omega_b} = 35, k_{\tau_6} = k_{\tau_7} = 0.9$.

Trajectory planning procedures were re-iterated for different choices of the base period T_0 in Eq. 23 ranging between 10 and 30 sec and, what is more important, *for different sets of kinematic parameters* of the KUKA LWR4+ either provided by the robot manufacturer for a generic set-up or obtained as a result of kinematics calibration discussed above. Examples of the 3-D path corresponding to excitation trajectories planned for Model 2 found for the set of calibrated kinematic parameters from Table 2 are

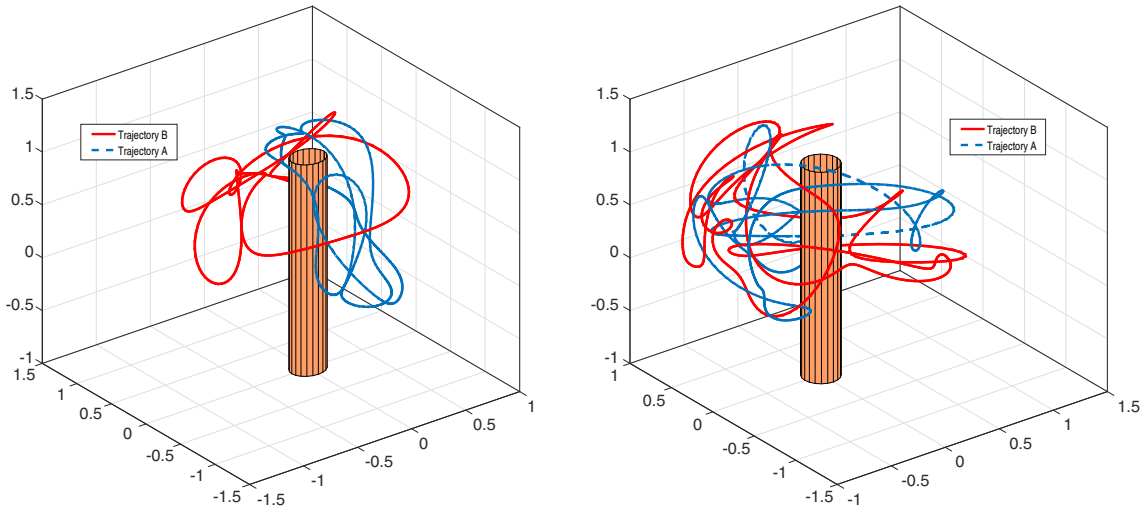

(a) $T_0 = 15sec$ (b) $T_0 = 25sec$

Fig. 5 Examples of excitation trajectories for dynamics calibration

shown in Fig. 5a, b. As seen, found trajectory candidates are "aggressive" and cover most of the robot workspace, but quite different from each other. More details on calibration trajectories planning, including trajectories characteristics obtained for different optimization strategies, can be found in authors' preceding work [27].

Dynamic parameters estimates were computed by Eq. 25. The outcomes of the implemented IDM identification procedure for different sets of kinematic parameters and types of calibration trajectories are presented on Fig. 6. Figure 7 illustrates how kinematic parameters influence the IDM identification results by showing the relative difference between essential dynamic parameters estimates obtained for CAD-based and calibrated MDH parameters values. Table 4 is matching numbers pointed in Figs. 6 and 7 with the names of corresponding essential parameters (see

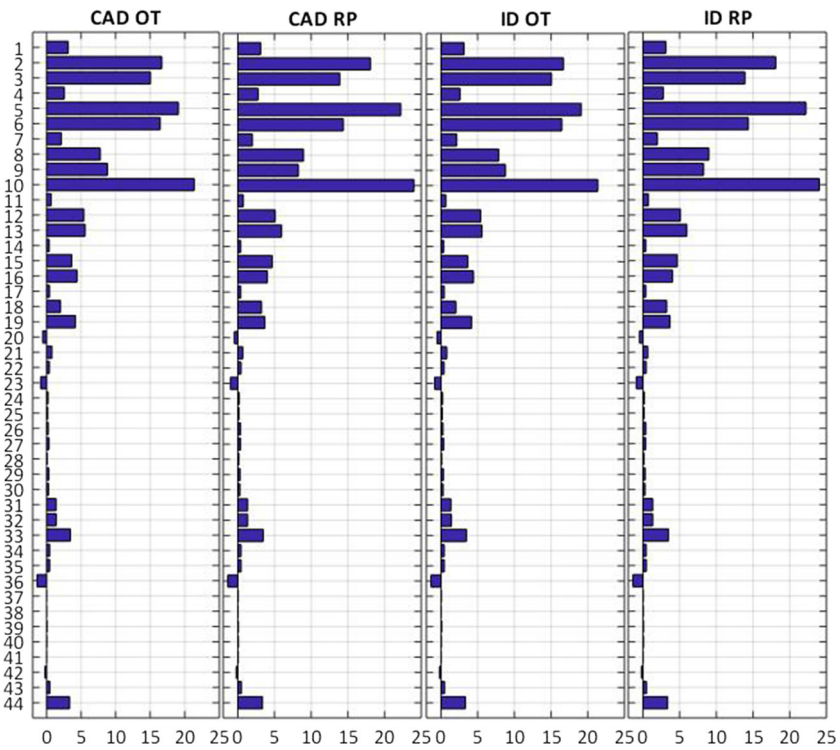

Fig. 6 Essential base parameters estimates for Model 2: CAD means CAD-based nominal estimates for kinematic (MDH) parameters, ID means calibrated kinematic parameters, RP stands for non-optimized calibration trajectory with 20 random way-points, OT stands for optimized Trajectory B with $T_0 = 25$ s

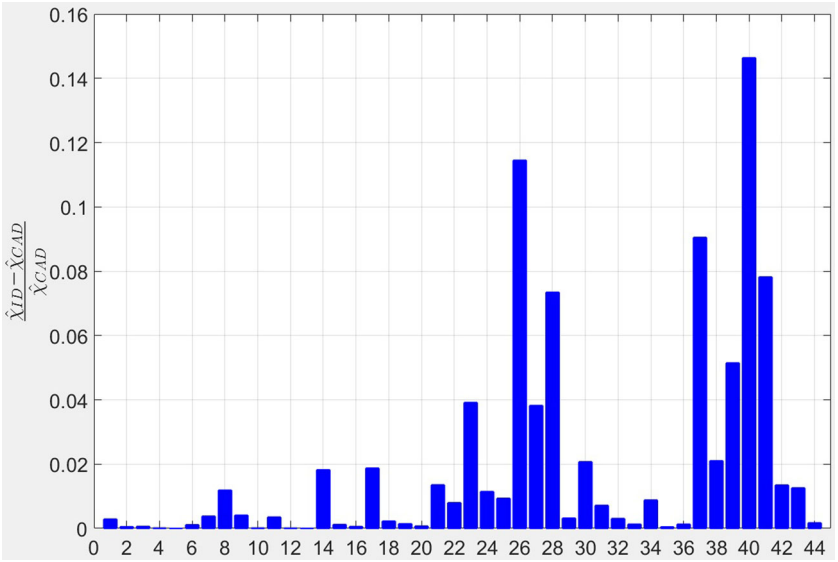

Fig. 7 Relative difference between essential parameters estimates obtained for Model 2 for CAD-based nominal (CAD) and calibrated (ID) kinematic parameters values

χ_j in Eq. 17), while R in index denotes that the parameter was obtained after regrouping.

Figure 8 shows results of the computed torque test performed to verify overall calibration accuracy that we can reach with multi-criterion calibration trajectory optimization and using advantageous of calibrated kinematic model. As one can see, even for a poorly loaded joint 6, absolute torque recovery error does not exceed 0.5 N m along most of the validation trajectory which is approximately 1% of the maximum torque value for the smallest joint.

6.3 General remarks

The most important outcomes and observations from the study are briefly commented next:

1. We proposed and verified several adjustments of a generic optimization based methods for robot calibration. This includes the argument to incorporate robot's kinematics parameters estimation as a prerequisite for calibration of dynamics and the argument on applicability and advantages of multi-objective constrained optimization in searching of excitation trajectories.

   To point out apparent advantages of the adjustments for organizing the identification, one can observe that we gained five to seven times improvement in positioning accuracy, while the difference between estimated and nominal MDH parameters is up to 1 mm in translation and more than 5° in rotational measures. Furthermore, with the proposed multi-objective optimization-based approach, we found feasible excitation trajectories with more uniform distribution of input signals for different joints specifically for the last three degrees of freedom q_5, q_6, and q_7. It resulted in shrinking the RSD of the IDM parameters' estimates twice if compared with corresponding values derived in [17].
2. As a separate contribution and for illustration purposes, such IDM identification procedure was applied for recovering the IDM of the KUKA LWR4+, where both of newly suggested points were realized in software and tested experimentally. Extended summary of qualitative results on estimating essential parameters for Models 1, 2, and 3 as well as its comparative analysis for

Table 4 Model 2 essential parameters

Num.	1	2	3	4	5	6	7	8	9	10	11
Param.	I_{a1}	$F_{vm,1}$	$F_{cm,1}$	I_{a2}	$F_{vm,2}$	$F_{cm,2}$	I_{a3}	$F_{vm,3}$	$F_{cm,3}$	$F_{vm,4}$	I_{a5}
Num.	12	13	14	15	16	17	18	19	20	21	22
Param.	$F_{vm,5}$	$F_{cm,5}$	I_{a6}	$F_{vm,6}$	$F_{cm,6}$	I_{a7}	$F_{vm,7}$	$F_{cm,7}$	$offm_7$	$F_{cl,1}$	$F_{cl,2}$
Num.	23	24	25	26	27	28	29	30	31	32	33
Param.	$offl_2$	$F_{cl,3}$	$F_{cl,4}$	$offl_4$	$F_{cl,5}$	$offl_5$	$F_{cl,7}$	$offl_7$	XX_{2R}	ZZ_{2R}	MY_{2R}
Num.	34	35	36	37	38	39	40	41	42	43	44
Param.	XX_{4R}	ZZ_{4R}	MY_{4R}	MY_{5R}	MY_{6R}	XX_8	YY_8	YZ_8	MY_8	MZ_8	M_8

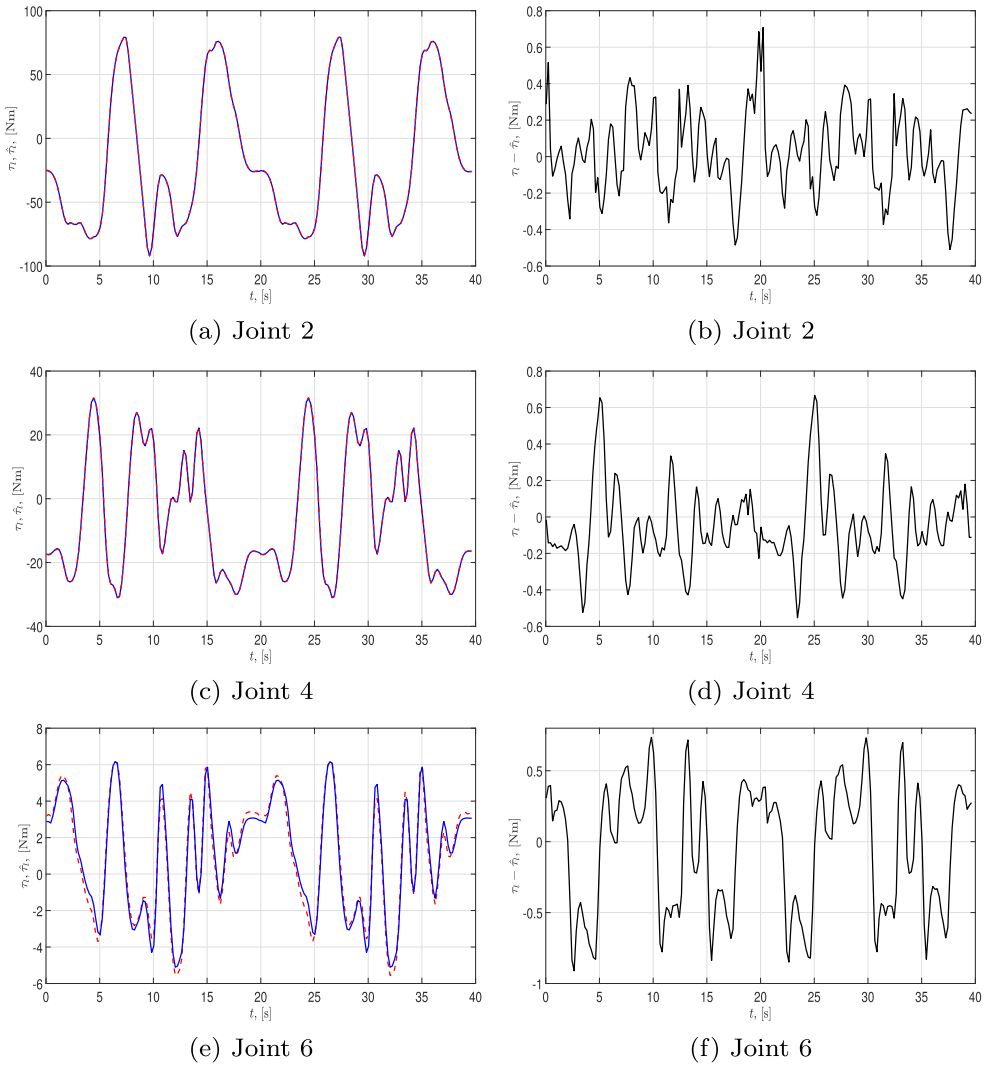

(a) Joint 2 (b) Joint 2

(c) Joint 4 (d) Joint 4

(e) Joint 6 (f) Joint 6

Fig. 8 IDM test: measured (solid blue) and computed (dotted red) joint torques, and its relative error (solid black)

different excitation trajectories and different choices of kinematic parameters can be found in the technical report attached as a supplementary material.

3. Another comparison of the results with [17] shows that KUKA LWR4+ robot-to-robot parameters variations can reach 20%. The biggest differences are related to friction coefficients and drive parameters, which can be explained by the influence from the internal and external wiring, manufacturing tolerances, and wear-and-tear. It can be also caused by the fact that in [17] non-calibrated kinematic parameters were used. The observation emphasizes importance of the sequential kinematic and dynamic calibration and proves that CAD-based parameters' values can only serve as rough estimates.

7 Conclusions and future work

The paper provides the comprehensive discussion of an integrated identification procedure, where the calibration of a robot dynamics becomes consistent with the calibration of its kinematic parameters. The work primarily illustrates the complexity of the problem and elucidates important details of use of measurement equipment, advanced symbolic and computational software tools, analytic formulations, and steps in integration work all required for developing a solution in the study.

However, there are a number of open problems. New identification approaches that can provide faster convergence under relaxed excitation conditions and handle measurements noise in a robust manner are required. In

this sense, the approach described in [1] looks a good alternative to the existing techniques. On the other hand, model accuracy verification methods should be advanced to derive a criterion reflecting minimum deviations in trajectories tracking tasks. Computed-torque tests do not give a direct answer to this question.

In any cases, found trajectories require syntheses of control systems. Successful examples and novel methods of feedback designs for orbital stabilization that complement the discussed model-based trajectory planning algorithms for underactuated as well as for fully actuated mechanical systems are recently reported in [32, 35].

References

1. Aranovskiy S, Bobtsov A, Ortega R, Pyrkin A (2016) Parameters estimation via dynamic regressor extension and mixing. Proc. of the American Control Conf July, 6971–6976
2. Bargsten V, Zometa P, Findeisen R (2013) Modeling, parameter identification and model-based control of a lightweight robotic manipulator. In: 2013 IEEE international conference on control applications (CCA), pp 134–139. https://doi.org/10.1109/CCA.2013.6662756
3. Bischoff R, Kurth J, Schreiber G, Koeppe R, Albu-Schaeffer A, Beyer A, Eiberger O, Haddadin S, Stemmer A, Grunwald G, Hirzinger G (2010) The kuka-dlr lightweight robot arm - a new reference platform for robotics research and manufacturing. In: Rob. (ISR), 2010 41st International Symposium on and 2010 6th German Conf. on Rob. (ROBOTIK), pp 1–8
4. Bobrow J, Dubowsky S, Gibson J (1985) Time-optimal control of robotic manipulators along specified paths. The Int J Rob Res 4(3):3–17
5. Briot S, Gautier M, Jubien A (2014) In situ calibration of joint torque sensors of the kuka lightweight robot using only internal controller data. In: 2014 IEEE/ASME international conference on advanced intelligent mechatronics, pp 470–475
6. Chen Q, Chen W, Yang G, Liu R (2013) An integrated two-level self-calibration method for a cable-driven humanoid arm. IEEE Trans Autom Sci Eng 10(2):380–391. https://doi.org/10.1109/TASE.2013.2242199
7. Gang C, Ton L, Ming C, Xuan JQ, Xu SH (2014) Review on kinematics calibration technology of serial robots. Int J Precis Eng Manuf 15(8):1759–1774
8. Daney D, Papegay Y, Madeline B (2005) Choosing measurement poses for robot calibration with the local convergence method and tabu search. The Int J Rob Res 24(6):501–518
9. Freidovich L, Robertsson A, Shiriaev A, Johansson R (2010) LuGre,-model-based friction compensation. IEEE Trans Control Syst Technol 18(1):194–200
10. Gautier M, Khalil W (1990) Direct calculation of minimum set of inertial parameters of serial robots. IEEE Trans Robot Automat 6(3):368–373
11. Gaz C, Flacco F, Luca AD (2014) Identifying the dynamic model used by the kuka lwr: a reverse engineering approach. In: 2014 IEEE Int. Conf. on Rob. and Automation (ICRA), pp 1386–1392
12. Gaz C, Flacco F, Luca AD (2016) Extracting feasible robot parameters from dynamic coefficients using nonlinear optimization methods. In: 2016 IEEE international conference on robotics and automation (ICRA), pp 2075–2081
13. Hollerbach J (1984) Dynamic scaling of manipulator trajectories. ASME J Dyn Syst Measurement, and Control 106(1):102–106
14. Hollerbach J, Khalil W, Gautier M (2008) Model identification. In: Siciliano B, Khatib O (eds) Springer Handbook of Rob. Springer, Berlin, pp 321–344
15. Hollerbach JM, Wampler CW (1996) The calibration index and taxonomy for robot kinematic calibration methods. The Int J Rob Res 15(6):573–591
16. Janot A, Vandanjon PO, Gautier M (2014) A generic instrumental variable approach for industrial robot identification. IEEE Trans Control Syst Technol 22(1):132–145
17. Jubien A, Gautier M, Janot A (2014) Dynamic identification of the Kuka LWR robot using motor torques and joint torque sensors data. IFAC Proc 19:8391–8396
18. Khalil W, Besnard S, Lemoine P (2000) Comparison study of the geometric parameters calibration methods. Int J Rob Auto 15(2):56–67
19. Khalil W, Creusot D (1997) SYMORO+: a system for the symbolic modelling of robots. Robotica 15(2):153–161
20. Khalil W, Dombre E (2004) Modeling, identification and control of robots. Elsevier Science
21. Khalil W, Gautier M (1991) Calculation of the identifiable parameters for robot calibration. In: The 9th IFAC/IFORS symposium on identification and system parameter estimation, pp 888–892. Budapest, Hungary
22. Khalil W, Gautier M, Enguehard C (1991) Identifiable parameters and optimum configurations for robots calibration. Robotica 9(01):63–70
23. Khalil W, Kleinfinger J (1986) A new geometric notation for open and closed-loop robots. In: Proceedings of 1986 IEEE Int. Conf. on Rob. and Automation, vol 3, pp 1174–1179
24. Khalil W, Lemoine P (1999) GECARO: a system for the geometric calibration of robots. APII-JESA European J Automation 33(5-6):717–739
25. Klodmann J, Lakatos D, Ott C, Albu-Schäffer A (2015) A closed-form approach to determine the base inertial parameters of complex structured robotic systems. IFAC-PapersOnLine 48(1):316–321
26. Kolyubin S, Paramonov L, Shiriaev A (2015) Robot kinematics identification: KUKA LWR4+ redundant manipulator example. J Phys Conf Ser 659(1):012,011
27. Kolyubin S, Shiriaev A, Jubien A (2017) Refining dynamics identification for co-bots: Case study on KUKA LWR4+. In: Preprints of the 20th IFAC World Congress, pp 15,191–15,196
28. Kolyubin SA, Paramonov L, Shiriaev AS (2015) Optimising configurations of KUKA LWR4+ manipulator for calibration with optical cmm. In: Bai S, Ceccarelli M (eds) Recent advances in mechanism design for rob., mechanisms and machine science, vol 33. Springer Int. Publishing, pp 189–199
29. Lehmann C, Olofsson B, Nilsson K, Halbauer M, Haage M, Robertsson A, Sörnmo O, Berger U (2013) Robot joint modeling and parameter identification using the clamping method. IFAC Proc pp 813–818
30. Marie S, Courteille E, Maurine P (2013) Elasto-geometrical modeling and calibration of robot manipulators: application to machining and forming applications. Mech Mach Theory 69:13–43
31. Nubiola A, Bonev IA (2013) Absolute calibration of an abb IRb 1600 robot using a laser tracker. Rob Comput Integr Manuf 29(1):236–245

32. Pchelkin S, Shiriaev A, Robertsson A, Freidovich L, Kolyubin S, Paramonov L, Gusev S (2017) On orbital stabilization for industrial manipulators: case study in evaluating performances of modified PD+ and inverse dynamics controllers. IEEE Trans Control Syst Technol 25(1):101–117
33. Rackl W, Lampariello R, Hirzinger G (2012) Robot excitation trajectories for dynamic parameter estimation using optimized b-splines. In: 2012 IEEE international conference on robotics and automation, pp 2042–2047
34. Renaud P, Andreff N, Lavest JM, Dhome M (2006) Simplifying the kinematic calibration of parallel mechanisms using vision-based metrology. IEEE Trans Robot 22(1):12–22
35. Shiriaev A, Freidovich L, Gusev S (2010) Transverse linearization for controlled mechanical systems with several passive degrees of freedom. IEEE Trans Autom Control 55(4):893–906
36. Stürz YR, Affolter LM, Smith RS (2017) Parameter identification of the kuka lbr iiwa robot including constraints on physical feasibility. IFAC-PapersOnLine 50(1):6863–6868
37. Swevers J, Ganseman C, Tukel D, de Schutter J, Brussel HV (1997) Optimal robot excitation and identification. IEEE Trans Robot Automat 13(5):730–740. https://doi.org/10.1109/70.631234